www.sciencedirect.com/journal/journal-of-vascular-nursing

Hemodynamic and structural effects on bypass graft for different levels of stenosis using fluid structure interaction: A prospective analysis

Md Shamsul Arefin

Although the flow dynamics have been investigated using fluid-structure interaction scheme for the internal thoracic artery–left anterior descending coronary artery (ITA-LAD) bypass graft in different cases, a detailed analysis associating different degrees of LAD stenosis and its effects on hemodynamics and structural displacement are not comprehensively studied. Therefore, the primary focus of this work is to examine and determine the correlation between the hemodynamic effects and structural variations inside the bypass graft with different degrees of LAD stenosis (0%, 30%, 50%, and 75%). Navier-Stokes equation, arbitrary Lagrangian-Eulerian, and elasticity in the solid region are implemented by coupling incompressible viscous fluid, nonlinear viscous fluid, and the stress tensor equations, respectively. Using fluid-structure interaction, variations in the hemodynamic property and changes in wall shear stress (WSS) including the spatial WSS distribution and the changes in the displacement of different degree of LAD stenosis are determined.Maximum WSS is found to be around 1.58E1 Pa near the anastomosis region and maximum magnitude for the structural displacement is found to be approximately 1.25E-5 m close to the heel. The results demonstrate that the disturbance in the flow pattern is evident mainly in the anastomosis region. Consequently, higher WSS is observed near the toe and on the artery wall, near the anastomosis region. (J Vasc Nurs 2019;37:169-187)

INTRODUCTION

The utilization of the internal thoracic artery (ITA) also known as internal mammary artery (IMA), comprising the left internal thoracic artery (LITA)-left anterior descending coronary artery (LAD) anastomosis increases the rate of subsistence of the patients. In addition, the LITA in coronary artery bypass grafting (CABG) is widely known because of its excellent/enduring patency rate.[1] The CABG technique has been very effective to re-establish the blood circulation in the moderate or completely blocked arteries.[2]

This technique uses either an autologous vein or any prosthetic channel/tube implanted into the nearest/proximal and remote/distal diseased section of the artery with the aim to re-establish the general circulation of the blood in myocardial infarction. The parameters for the hemodynamic forces, for instance, wall shear stress (WSS) applied on the endothelial cells, oscillatory shear index, and temporal or spatial WSS gradient are the most substantial features, which can manipulate the patency of CABG. Today, most usual operative process for the myocardial revascularization comprises an ITA combined with one or more saphenous vein grafts. To increase the rate of survival of the patients, the LAD comprising an ITA needs to be supplied without any obstruction.[2–5] Sabik et al 2013, studied the effect of CABG after the reoperation using the LITA grafting LAD for the patients and they declared that the reoperation is harmless alongside with the discussion of risk included survival benefit.[6]

Consequently, the hemodynamic studies of the CABG have been extensively analyzed by using the computational fluid dynamics (CFD), which determines the fluids behavior, including particle image velocimetry measurements so that the flow pattern found using the numerical models could be verified.[7–9] The combination of these schemes permits successful identifications of several factors for instance, blood flow fields, WSS and gradients, deformation of the artery and graft junction including the degree of compliance divergence. Moreover, using fluid-structure interaction (FSI) for the bypass graft, simulations have been carried out by Kouhi et al 2008 and Do, 2012.[10,11] FSI involves the fluid and structure interaction, which mimics the real-time scenario of the model condition (eg, CABG grafting, cardiac flow simulation, aneurysm, and so forth) by coupling the fluid dynamics and structural mechanics laws. Furthermore, the CFD technique has also been used by Ethier et al 1998 and the researchers stated that the low and oscillatory WSS regions are the critical locations for the intimal hyperplasia and frequently spotted in distal anastomosis.[12] In addition, by using CFD, Goubergrits et al, 2001,

From the FSET, Swinburne University of Technology, Hawthorn, Victoria, Australia.

Corresponding author: Md Shamsul Arefin, FSET, Swinburne University of Technology, Hawthorn, Victoria 3122, Australia (E-mail: arefin_16bd@yahoo.com).

Conflict of interest: None.

1062-0303/$36.00

https://doi.org/10.1016/j.jvn.2019.05.006

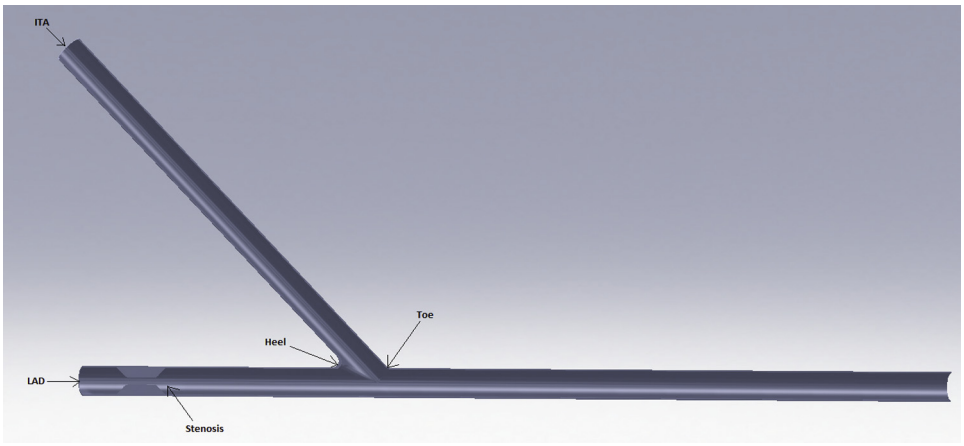

Figure 1. *Cross-section of the ITA-LAD bypass graft (SolidWorks, 2012). ITA-LAD = internal thoracic artery–left anterior descending coronary artery.*

determined the significance of the low WSS area in graft-failure into a saphenous vein and a varicose saphenous vein.[13]

In another research, using CFD Freshwater et al, 2006, investigated the impact of the anastomosis angles on the WSS and flow profiles of the left internal mammary artery–LAD bypass model. During the study, the physiological effects of the bypass graft have been neglected.[7] In the same year, Sankarnarayanan et al 2006 examined the flow pattern for a CABG graft model (out-of-plane) by using the CFD and the researchers found substantial effects which can influence the patency of the graft. However, the influence of the elasticity has not been considered.[14]

Due to the complexity of the coupled FSI scheme, the computational and experimental researches of CABG mainly assessed the hemodynamic relation between the force and inflexible arterial wall,[15–21] but this statement is only applicable for those circumstances where the fluid flow is not affected by any physiological deformation of the structure.[2,22] Moreover, Frauenfelder et al, 2007, examined the flow pattern and WSS for the end-to-side and side-to-side anastomosis of the CABG using CFD.[23] Afterward, Nordgaard et al, 2010, examined the effects of competitive flow by using CFD on WSS in the left internal mammary artery–LAD bypass grafts of the porcine model and they concluded that the flow characteristics into the graft is extremely reliant on the degree of competitive flow.[24]

Subsequently, Berger et al, 2004, examined the effect of clinical and angiographic factors and specifically the effect of the degree of stenosis on the local vessel. They investigated the correlation between the long-lasting patency of the IMAs with clinical and angiographic data. Although certain restrictions have been applied on the patients, they have found that the long-term patency rate is minimal if the receiver's vessel is reasonably stenosed.[25] Moreover, the fluid flow in the CABG of a patient-specific model has been simulated by Sankaran et al, 2012, by using an implicitly coupled multiscale model to carry out CFD simulation.[26]

Later, Morsi et al, 2012, simulated the directional movement of the artery for the total mesh displacement and mesh velocity distributions comprising the WSS and velocity vectors of a

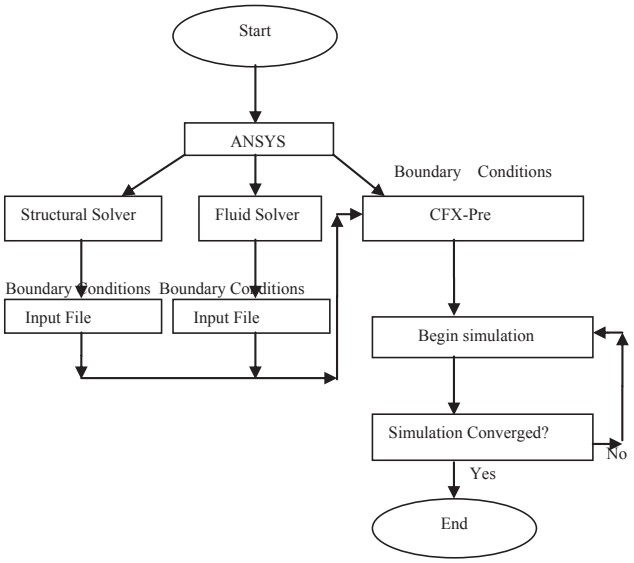

Figure 2. *Demonstration of the ITA-LAD simulation process. ITA-LAD = internal thoracic artery–left anterior descending coronary artery.*

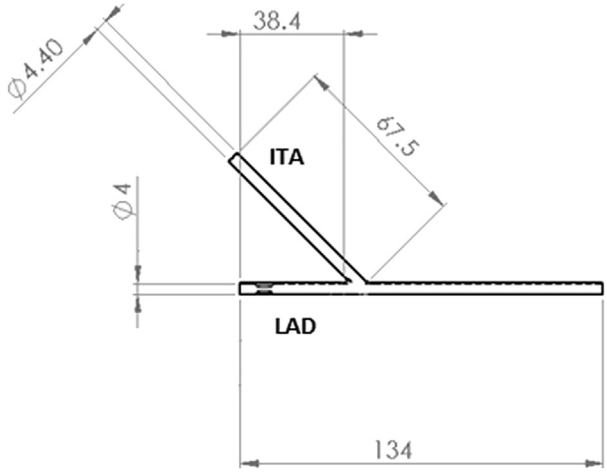

Figure 3. *Cross-section of an ideal ITA-LAD bypass graft (SolidWorks, 2012). ITA-LAD = internal thoracic artery–left anterior descending coronary artery.*

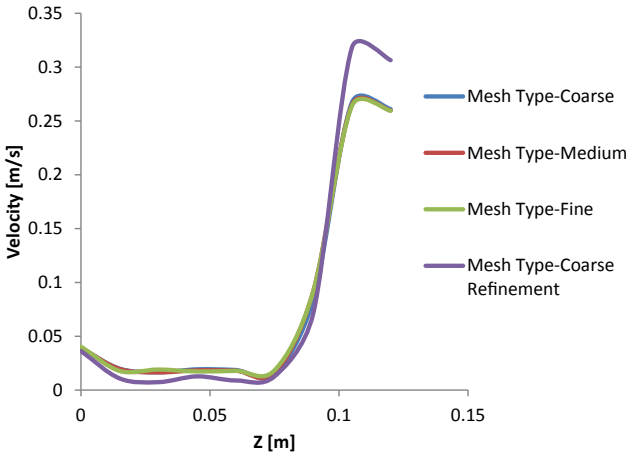

Figure 4. *Mesh independency test using line control properties on fluid velocity.*

bypass graft of 20° anastomosis angle with the graft-artery ratio of 1.6 during the peak systole. Results demonstrated for the first time, the maximum deformation region and the direction of motion of the CABG during one cardiac cycle. The researchers mentioned that the outcomes could be very useful for the surgeons and the graft designers, which also comprises the selection of biomaterials. They also stated that computation using FSI-coupling technique is also significant to obtain the deformation, which can certainly affect the total results.[27] After that, Kabinejadian and Ghista, 2012, introduced a novel design of CABG comprising the side-to-side and end-to-side anastomoses. From the results, when compared with the regular end-to-side anastomoses, the design might enhance the patency rate of the CABG than the usual. During the entire simulations, two-way FSI technique has been used.[28] However, Siddiqui et al, 2009, studied the pulsatile blood flow in a stenosed artery where the blood was modeled similar to the Casson fluid, and they have

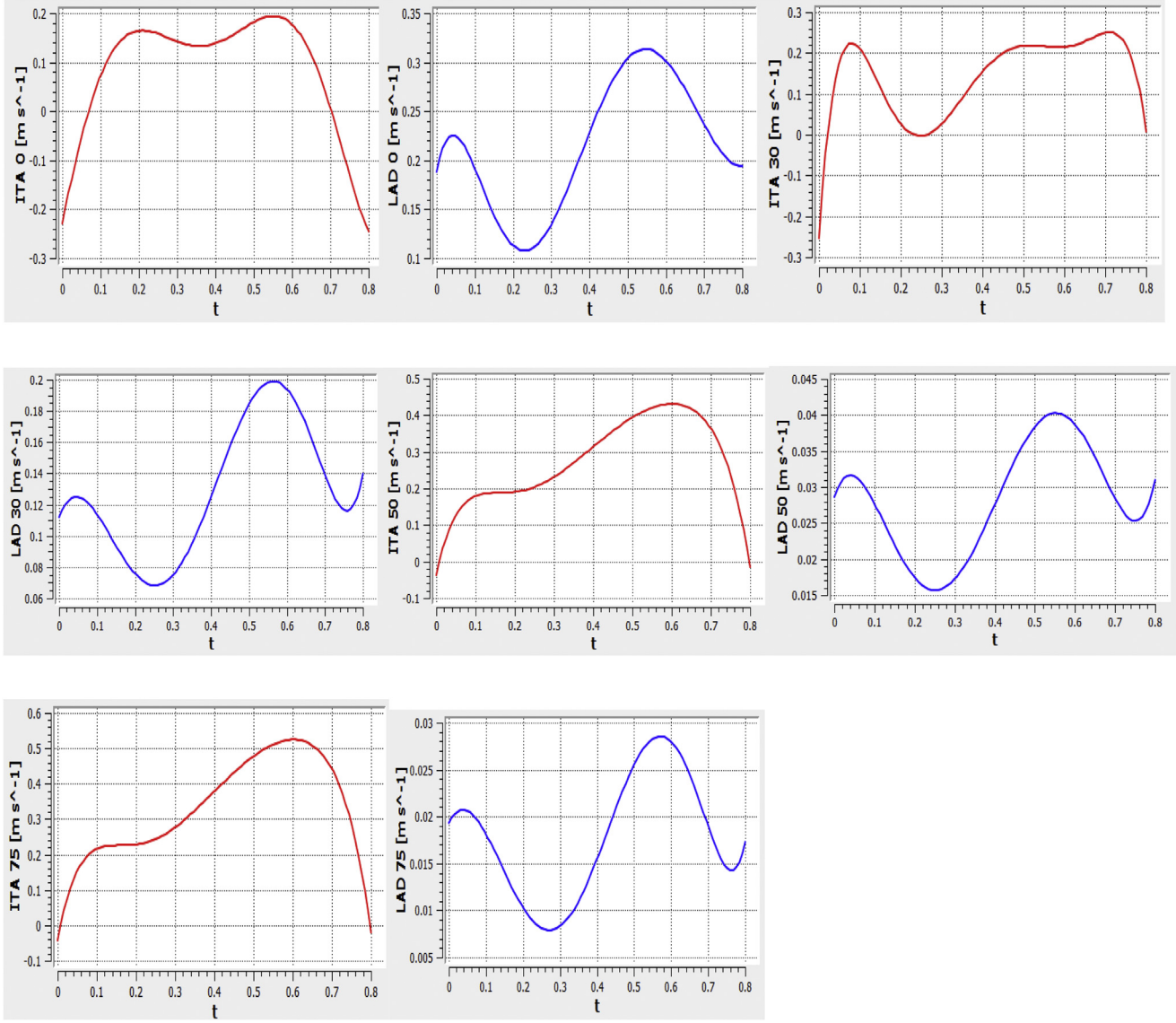

Figure 5. *Inlet velocities for different degree of stenosis in the ITA-LAD bypass graft (t is in seconds).*[30] *ITA-LAD = internal thoracic artery–left anterior descending coronary artery.*

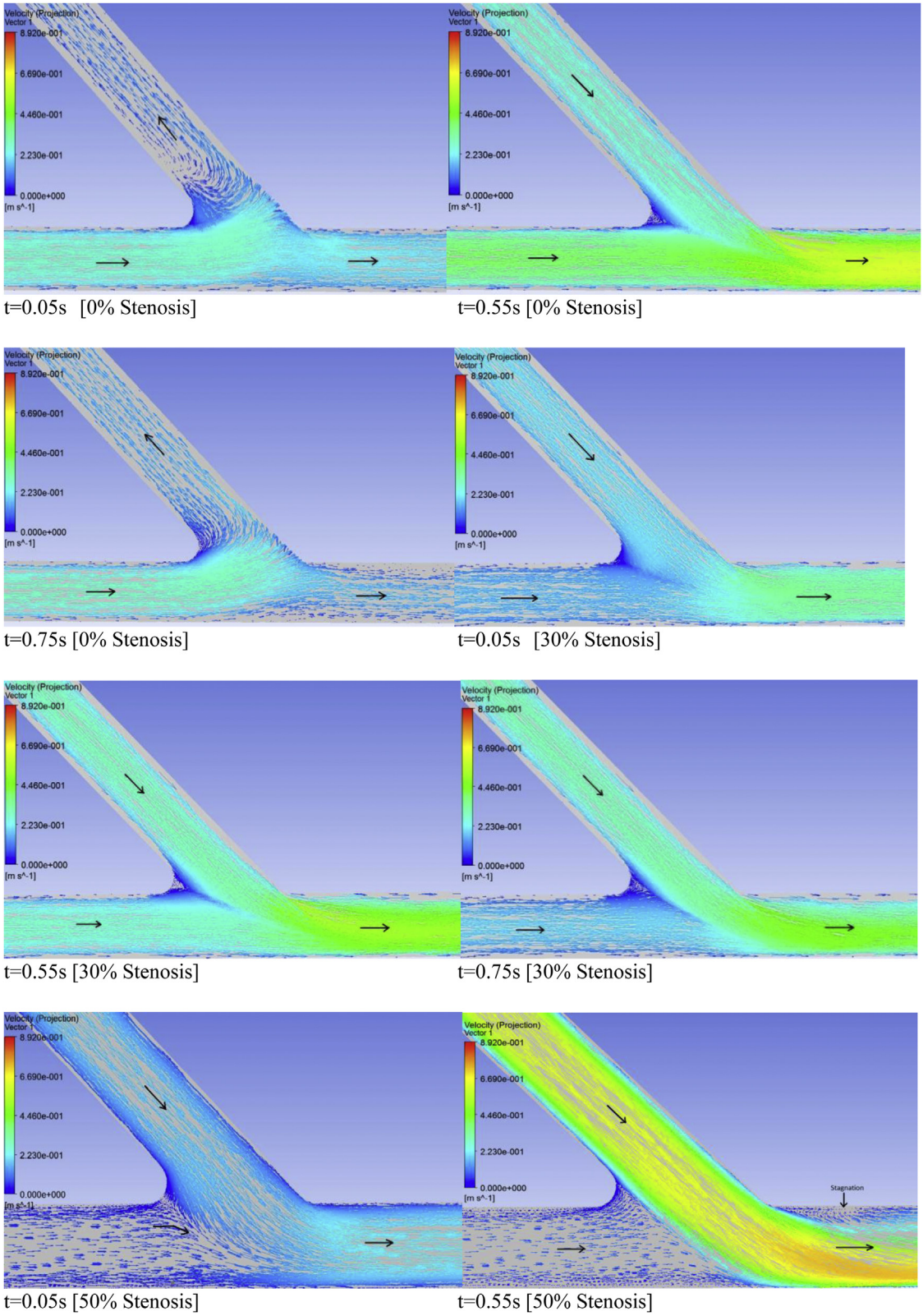

Figure 6. *Velocity distribution of ITA-LAD bypass graft for different stenosis. ITA-LAD = internal thoracic artery–left anterior descending coronary artery.*

concluded that their model could be useful to analyze the blood flow during the disease phase and the blood behaves like non-Newtonian fluid.[29]

Later on 2012, Ding et al, 2012, studied the effect of competitive flow on hemodynamics for the in vivo experiment of 18 pigs in the ITA-LAD model based on the different stenosis values on

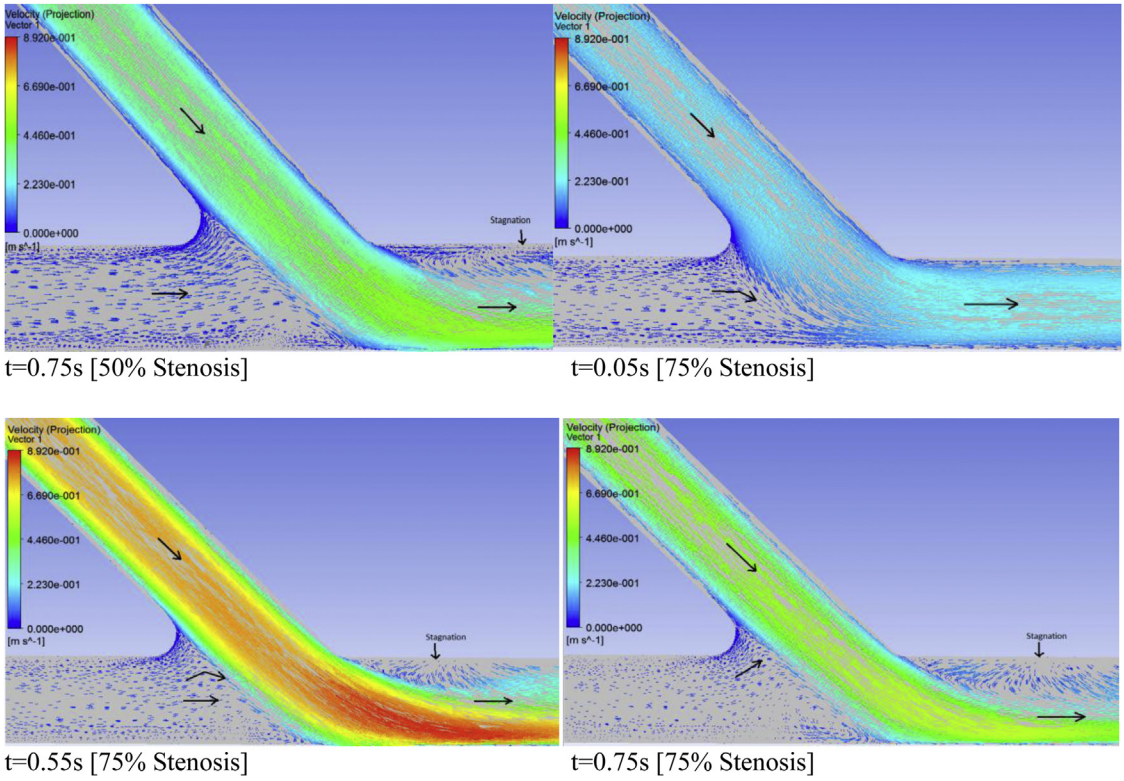

Figure 6. *(*continued*).*

the LAD. During the simulations, only CFD technique has been used but no FSI effects have been considered.[30] Afterward, Lassila et al, 2013, investigated the hemodynamic inverse problem using the bypass graft.[31]

Although the aforementioned studies mainly focused on the overall flow pattern inside the CABG with different degrees of accomplishment, a complete analysis related to hemodynamics and physiological variations inside the bypass graft, by varying the degree of LAD-stenosis (0%, 30%, 50%, and 75%), is not thoroughly analyzed. Therefore, this article aims to investigate and determine the correlation between the degree of LAD stenosis and the hemodynamic effect and structural effect by using FSI under various physiological conditions. More precisely, changes in the direction of flow patterns including the disturbance and separation of flows in the anastomosis angle and WSS incorporating spatial WSS distribution are fully investigated for the bypass graft (Figure 1). Moreover, structural deformation is determined in terms of total mesh displacement for varying degree of LAD stenosis.

MATHEMATICAL APPROACHES

The ANSYS software system is used to solve the 3D time-dependent equations, which depends on the finite volume method and different coupled iterative solver equations. The fluid flow complications are basically explained by using the laws of conservation of mass, momentum, and energy equations. All these principles are stated in the form of partial differential equations, and these equations are then discretized using the finite element–based approach. Hence, the Navier-Stokes equation characterizing the time-dependent incompressible viscous fluid coupled with the continuity equation is utilized in the entire simulations.[32,33]

$$\frac{\partial p}{\partial y}+\frac{\partial(\rho \mathrm{Vx})}{\partial x}+\frac{\partial(\rho \mathrm{Vy})}{\partial y}+\frac{\partial(\rho \mathrm{Vz})}{\partial z}=0 \tag{1}$$

The momentum equations are[32,33]

$$\begin{aligned}&\frac{\partial \rho v_x}{\partial t}+\frac{\partial(\rho v_x v_x)}{\partial x}+\frac{\partial\left(\rho v_y v_x\right)}{\partial y}+\frac{\partial(\rho v_z v_x)}{\partial z}\\&\quad=\rho g_x-\frac{\partial P}{\partial x}+R_x+\frac{\partial}{\partial x}\left(\mu_e \frac{\partial v_x}{\partial x}\right)+\frac{\partial}{\partial y}\left(\mu_e \frac{\partial v_x}{\partial y}\right)\\&\qquad+\frac{\partial}{\partial z}\left(\mu_e \frac{\partial v_x}{\partial z}\right)\end{aligned} \tag{2}$$

$$\begin{aligned}&\frac{\partial \rho v_y}{\partial t}+\frac{\partial\left(\rho v_x v_y\right)}{\partial x}+\frac{\partial\left(\rho v_y v_y\right)}{\partial y}+\frac{\partial\left(\rho v_z v_y\right)}{\partial z}\\&\quad=\rho g_y-\frac{\partial P}{\partial y}+R_y+\frac{\partial}{\partial x}\left(\mu_e \frac{\partial v_y}{\partial x}\right)+\frac{\partial}{\partial y}\left(\mu_e \frac{\partial v_y}{\partial y}\right)\\&\qquad+\frac{\partial}{\partial z}\left(\mu_e \frac{\partial v_y}{\partial z}\right)\end{aligned} \tag{3}$$

TABLE 1

VELOCITY MAPPING OF THE BYPASS GRAFT FOR DIFFERENT DEGREES OF LAD STENOSIS

Degree of Stenosis	*Results*
0%	For the 0% stenosis/no stenosis condition, the initial velocity for the ITA and LAD artery are 0 m/second and around 0.23 m/second, respectively (t = 0.05 seconds), and a reverse-flow/flow separation is observed into the graft artery (ITA). Consequently, during the time step of t = 0.55 seconds, the magnitude of the inflow jet through the ITA increased to around 0.19 m/second. At the same time, the inflow jet through the proximal LAD region elevates the magnitude of the velocity and maximum magnitude is found to be approximately 6.69E-1 m/s near the anastomosis angle in the distal LAD. Again, with the deceleration in the inflow jet coming from the ITA (around −0.18 m/second) and LAD (around 0.22 m/second), a reverse flow pattern is found to be in the ITA region.
30%	With the time step of t = 0.05 seconds, the magnitude of the inflow velocity in the LAD and ITA region are found to be approximately 0.13 m/second and 0.15 m/second, respectively. Because of the stenosis in the proximal LAD region, disturbance in the flow profile is seen in the anastomosis region, close to the heel. In addition, the flow is found to be in the forward direction. Again, with the time step of t = 0.55 seconds, the velocity of the inflow wave increases to around 0.225 m/second through the ITA region and hence maximum magnitude of velocity of approximately 6.69E-1 m/s is found besides the anastomosis area of the distal LAD. Subsequently, with the time step of t = 0.75 seconds, much higher magnitude of velocity is found for the ITA (0.22 m/second) compared with the LAD (0.12 m/second). Therefore, the magnitude of the fluid velocity around 4.46E-1 m/s is found to be near the artery wall of the LAD.
50%	With the time step of t = 0.05 seconds, the velocity of the ITA and LAD region is found to be approximately 0.13 m/second and 0.031 m/second, respectively. As the degree of stenosis in the LAD region increases, the magnitude of the velocity in the LAD area decreases. In addition, a disturbance in the flow pattern is seen in the anastomosis region. Subsequently, during the time step of t = 0.55 seconds, the magnitude of the inlet waveform rises through the ITA region (around 0.42 m/second) than its LAD region (0.04 m/second). At the same time step, maximum magnitude of approximately 7.33E-1 m/s flow velocity is observed near the artery wall of the distal LAD. Conversely, with the decrease in the velocity through the ITA region (approximately 0.2 m/second) (t = 0.75 seconds), disturbance in the flow dynamics is seen, which includes the recirculation/formation of ring-shaped vortex near the surrounding area of the anastomosis region.
75%	The inlet velocity with the value of approximately 0.021 m/second for the 75% LAD stenosis and a feeble ring-shaped vortex is observed close to the surrounding area of the anastomosis region of the arterial wall. Consequently, through the ITA region, the magnitude of the inflow velocity (0.52 m/second) is found to be increased and hence maximum magnitude of around 8.92E-1 m/s is found to be near the artery wall of the distal area. After that, during the time step of t = 0.75 seconds, the magnitude of the ITA is found to be decelerated with the value of approximately 0.25 m/second. At the same time, a disturbance is seen in the anastomosis region where a ring-shaped vortex is developed in the surrounding area of the arterial wall.

ITA-LAD = internal thoracic artery–left anterior descending coronary artery.

$$\frac{\partial \rho v_z}{\partial t} + \frac{\partial (\rho v_x v_z)}{\partial x} + \frac{\partial (\rho v_y v_z)}{\partial y} + \frac{\partial (\rho v_z v_z)}{\partial z} = \rho g_z - \frac{\partial P}{\partial z} + R_z + \frac{\partial}{\partial x}\left(\mu_e \frac{\partial v_z}{\partial x}\right) + \frac{\partial}{\partial y}\left(\mu_e \frac{\partial v_z}{\partial y}\right) + \frac{\partial}{\partial z}\left(\mu_e \frac{\partial v_z}{\partial z}\right) \quad (4)$$

V_x, V_y, and V_z are denoted as the velocity vector components in the direction of X, Y, and Z accordingly, and ρ represents the density of the fluid, whereas μ represents the viscosity of the fluid, and x, y, and z represent the global Cartesian coordinates. R_x, R_y, and R_z represent the distributed resistance, which is generally used to model the impact of geometric features excluding the model.

The motion equation for the elastic in the solid domain is[33,34]

$$\Delta \cdot \sigma + f = 0 \quad (5)$$

where, σ denotes the stress tensor and f is the body force.

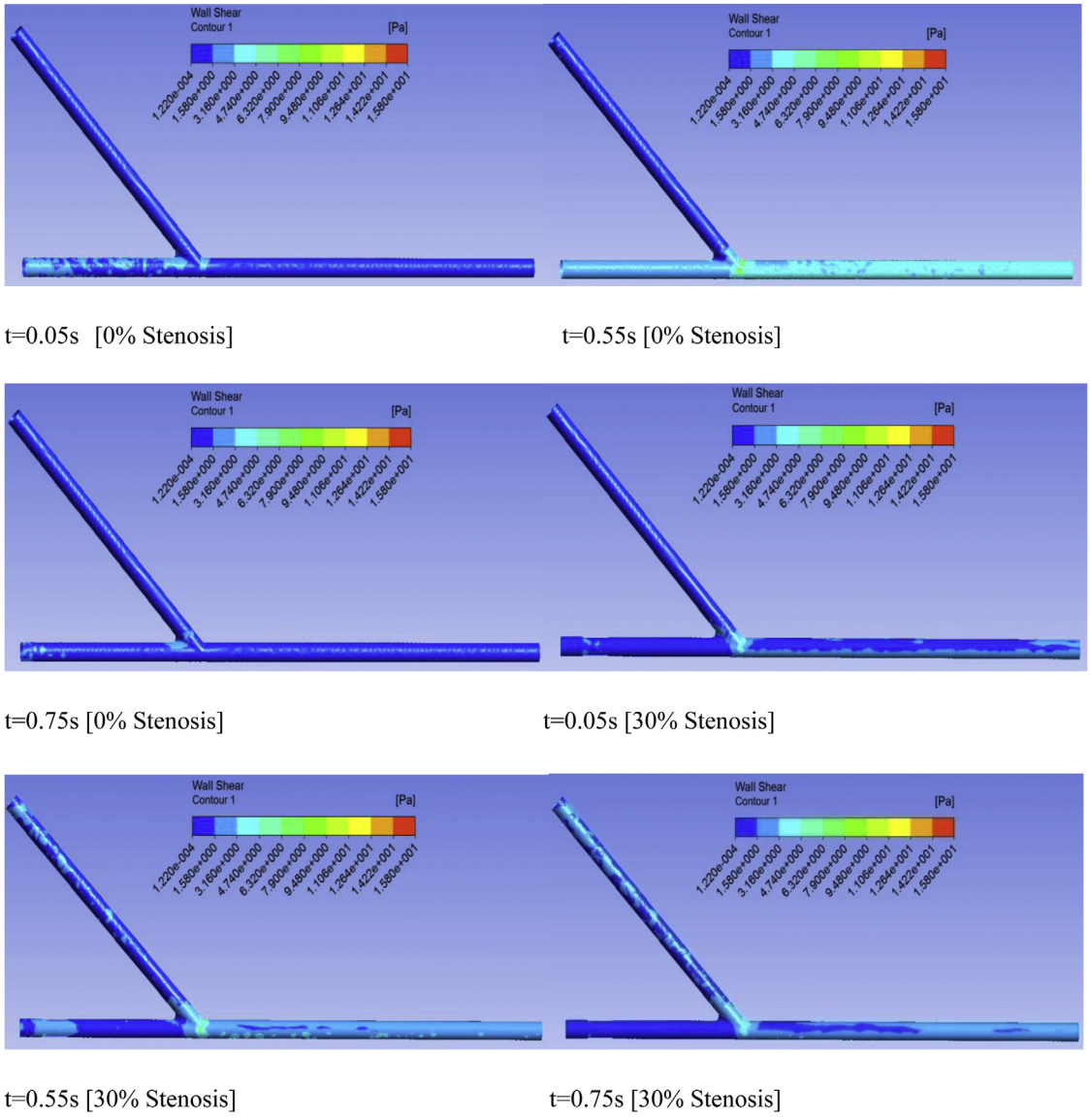

Figure 7. *Wall shear stress distribution for the ITA-LAD bypass graft based on degree of LAD stenosis. ITA-LAD = internal thoracic artery–left anterior descending coronary artery.*

In addition, small deformation is presumed and the equation for the stress is[33,34]

$$\sigma = \frac{E}{1+\upsilon}\left(\frac{v}{1-2\upsilon}\mathrm{tr}(\varepsilon)I + \varepsilon\right) - \frac{E}{1-2\upsilon}\alpha(T - T_0)I \qquad (6)$$

E is the Young's modulus, υ is the Poison's ratio, T denotes the temperature, T_0 is the reference temperature, and I denotes unit tensor.

During the simulations, arbitrary Lagrangian-Eulerian (ALE) finite-element method is used to compute the viscous fluid, which is nonlinear. When comparing to the Eulerian method, ALE presents much accurate result for the deformable structure that comprises fluid. The Eulerian method is efficient for the nondeformed/fixed boundary conditions, whereas the ALE method is more fitting for the deformed/moving boundary conditions.[33] Comprehensive description can be found for the Navier-Stokes equation and ALE formulation in the studies by Temam, Souli et al, Huerta and Liu, and Donea et al.[32,35–37] Semi-Implicit Method for Pressure-Linked Equations (SIMPLE) algorithm is applied to compute the mass and momentum equations used in the current simulations.[33,38,39] Figure 2 demonstrates the FSI algorithm in terms of a flow chart for the entire simulation.

ANSYS 14.5 is used for the simulation and during computational approach, subsequent steps are followed: first, the required features are assigned to the specific geometry, which comprises the material density and appropriate isotropic characteristics. Second, the meshing is computed by using the ALE formulation and finally, depending on the conditions, coupling procedure is selected, where the coupled time steps are provided using numerical time steps/values or by using the adaptive method. The total time duration for the simulation is considered 0.8 seconds.[30]

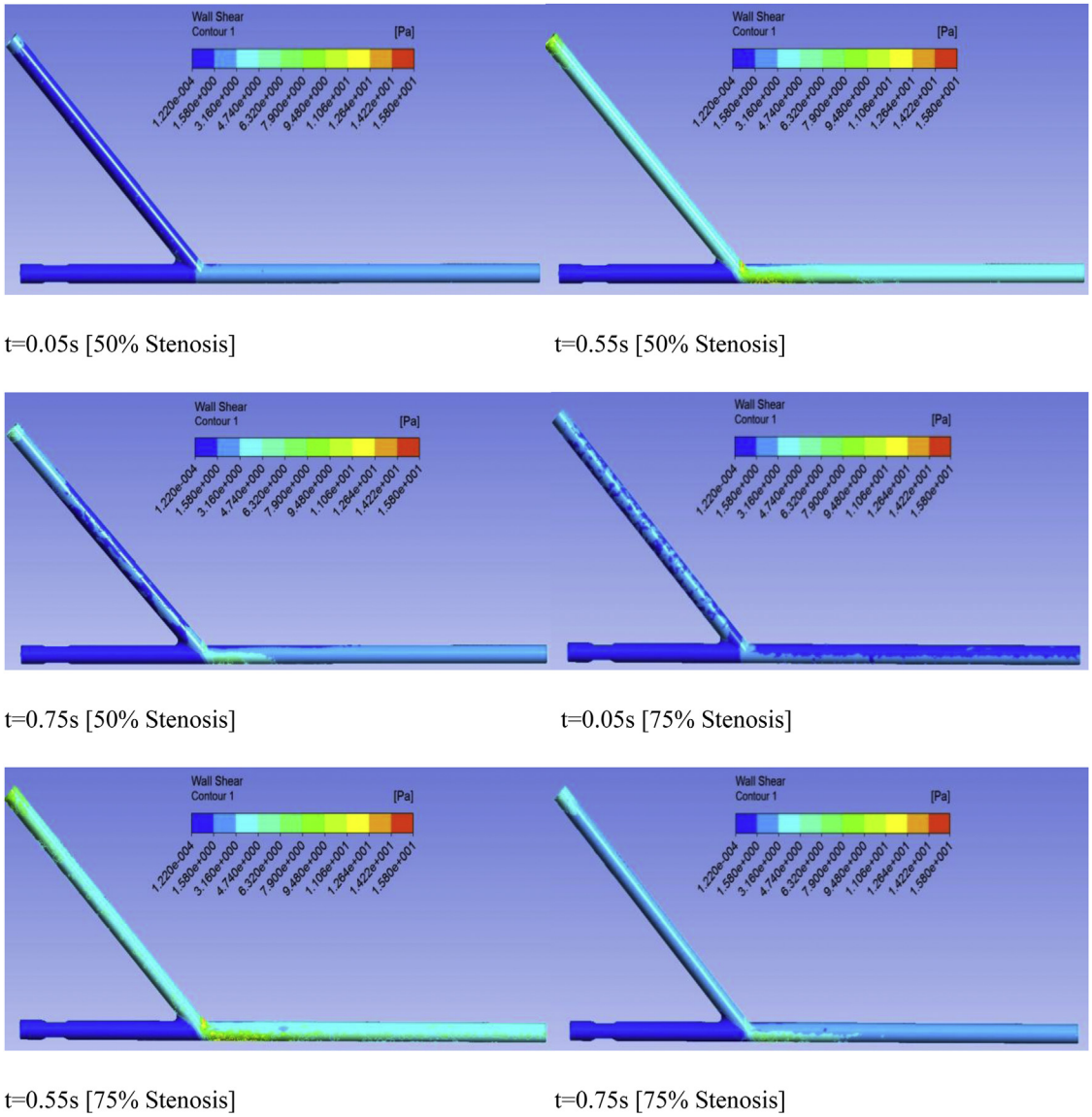

Figure 7. *(*continued*).*

COMPUTATIONAL PROCEDURE

Geometric construction

An ideal CABG model is demonstrated in Figure 3 (SolidWorks, 2012).

In the ITA-LAD bypass graft, the length of the native stenosed LAD is taken 134 mm, and the length of the anastomosed ITA is 67.5 mm. The diameters of the ITA and LAD are 4.40 mm and 4 mm, respectively. The anastomosis angle is 45° for all the simulations. Figure 3 exhibits the cross-section of a general ITA-LAD graft, which is used for the remedy of LAD stenosis.[2,30]

Meshing configurations and mesh independency test

The geometry of the bypass graft is then introduced into ANSYS 14.5, and required meshing is executed along with the necessary boundary condition to compute the simulations. Mapped face meshing is generated separately both for the solid and fluid regions. Subsequently, the mesh independency testing is carried out using the line control properties by comparing the changes in fluid velocity for subsequent nodes and elements until the changes in velocity are saturated (Figure 4).[2] Four different types of mesh statistics (coarse, medium and fine and coarse refinement) are used and changed during the testing. Results showed that 19,706 nodes and 10,058 elements are suitable for the solid and 138,311 nodes and 746,829 elements are suitable for the fluid regions. These nodes and elements are attained for the medium mesh type. Moreover, the convergence criterion for the fluid flow profile is considered 10^{-4}, and the value is considered 10^{-2} for the coupling data transfer.[33]

Boundary conditions

The blood flow velocity profiles/inlet velocity waveforms are taken from the in vivo trials of 18 pigs as reported in the study by Ding et al. Based on the stenosis in LAD, different inlet profiles are demonstrated in Figure 5. Four different degrees of LAD

TABLE 2

WSS DISTRIBUTIONS OF THE BYPASS GRAFT FOR DIFFERENT DEGREES OF LAD STENOSIS

% Stenosis	*Observations*
0%	During the time step of t = 0.05 seconds, the magnitude of the WSS is observed to be moderately higher near the inlet region (LAD) and the toe. Because of higher inflow velocity through the LAD than ITA, the magnitude of the WSS is observed to be slightly higher in the LAD. After that, with the time step of t = 0.55 seconds, the magnitude of the inflow velocity increased again and therefore, WSS (approximately 7.9 Pa) is found to be in the distal LAD area. Again, with t = 0.75 seconds, the inflow velocities through the ITA and LAD area decelerated, and therefore, the magnitude of the WSS is observed to be lower compared with its previous time step.
30%	Once again, with the time step of t = 0.05 seconds, lower inlet velocities coming through the inlet regions and moderately higher WSS is observed to be close to the toe. Subsequently, with the time step t = 0.55 seconds, WSS is observed to be somewhat higher on the distal LAD region, as the inflow velocities are higher through the LAD and ITA. During this time step, maximum magnitude is observed to be approximately 6.32 Pa near the toe. Later, higher WSS is still observed to be in the toe region because of higher inflow velocity entered through the ITA (t = 0.75 seconds).
50%	With the time step of t = 0.05 seconds, lower WSS is observed to be on the ITA and proximal LAD, but higher WSS is observed to be on the distal LAD region. This is due to the lower inlet velocities entered through the ITA and LAD regions. Subsequently, with the time step of t = 0.55 seconds, much higher magnitudes of WSS are observed to be on the distal LAD, ITA, and anastomosis area. This can be explained that with higher magnitude of inflow wave entered through the ITA region, WSS increased, and at the same time, the magnitude raised on the anastomosis area and on the host artery. WSS with the value of approximately 1.58E1 Pa is observed to be near the anastomosis area. Later, with the time step of t = 0.75 seconds, lower magnitude of WSS is observed to be on the inlet of ITA and distal LAD as the inflow velocities decreases, when compared with its previous time step.
75%	Because of minimal inflow waveforms, slightly higher magnitude of WSS is found to be on the ITA region compared with its proximal LAD (t = 0.05 seconds). Consequently, with the increase in the rate of flow through the ITA, WSS is found to be higher on the distal LAD, ITA, and anastomosis area. Maximum WSS with the value of approximately 1.42E1 Pa is observed to be close to the anastomosis area on the distal LAD. Afterward, with the time step of t = 0.75 seconds, the inflow waveform through the ITA and LAD area decelerated and hence WSS graft artery and on the distal LAD consisting the anastomosis area is found to be decreased as well.

ITA-LAD = internal thoracic artery–left anterior descending coronary artery; WSS = wall shear stress.

stenosis, 0% or no stenosis, 30%, 50%, and 75% stenosis are considered during the simulations.

Subsequently, the native wall of the artery is assumed to be isotropic and homogeneous. Newtonian fluid flow is considered for this simulation, where the density of the fluid and fluid viscosity are considered to be 1,050 kg/m^3 and 0.0035 Pa s, respectively. In addition, the flow is considered to be laminar. Moreover, in the outlet region, relative pressure is considered to be 0 Pa and the Poisson's ration is considered to be 0.49.[2,30,40] Furthermore, the under-relaxation factor is provided with the value of 0.75. Young's modulus is computed from the following equation[2,41]:

$$\frac{Eh}{r_0} = k_1 \times \exp(k_2 r_0) + k_3 \quad (7)$$

Where, r_0 represents the distal area artery diameter, h is the wall thickness, the constants with the value of $k_1 = 2 \times 10^7$ g/s^2 cm, $k_2 = -22.53$ cm^{-1}, and $k_3 = 8.652 \times 10^5$ g/s^2 cm.

Consequently, the inlet velocities are given below for different LAD stenosis, where the x-axis contains the time (s) and y-axis contains the velocity (m/s). The velocities are curve-fitted with the inlet velocities from Ding et al, 2012, which are in good match apart from LAD 50% (because of the variation in inlet velocities).[30] Moreover, due to different inlet velocities for different degree of LAD stenosis (as obtained from Ding et al, 2012), a cylindrical support on the bypass graft has been used. Hence, it slightly restricts the displacement of the bypass graft, especially for higher levels of LAD stenosis.

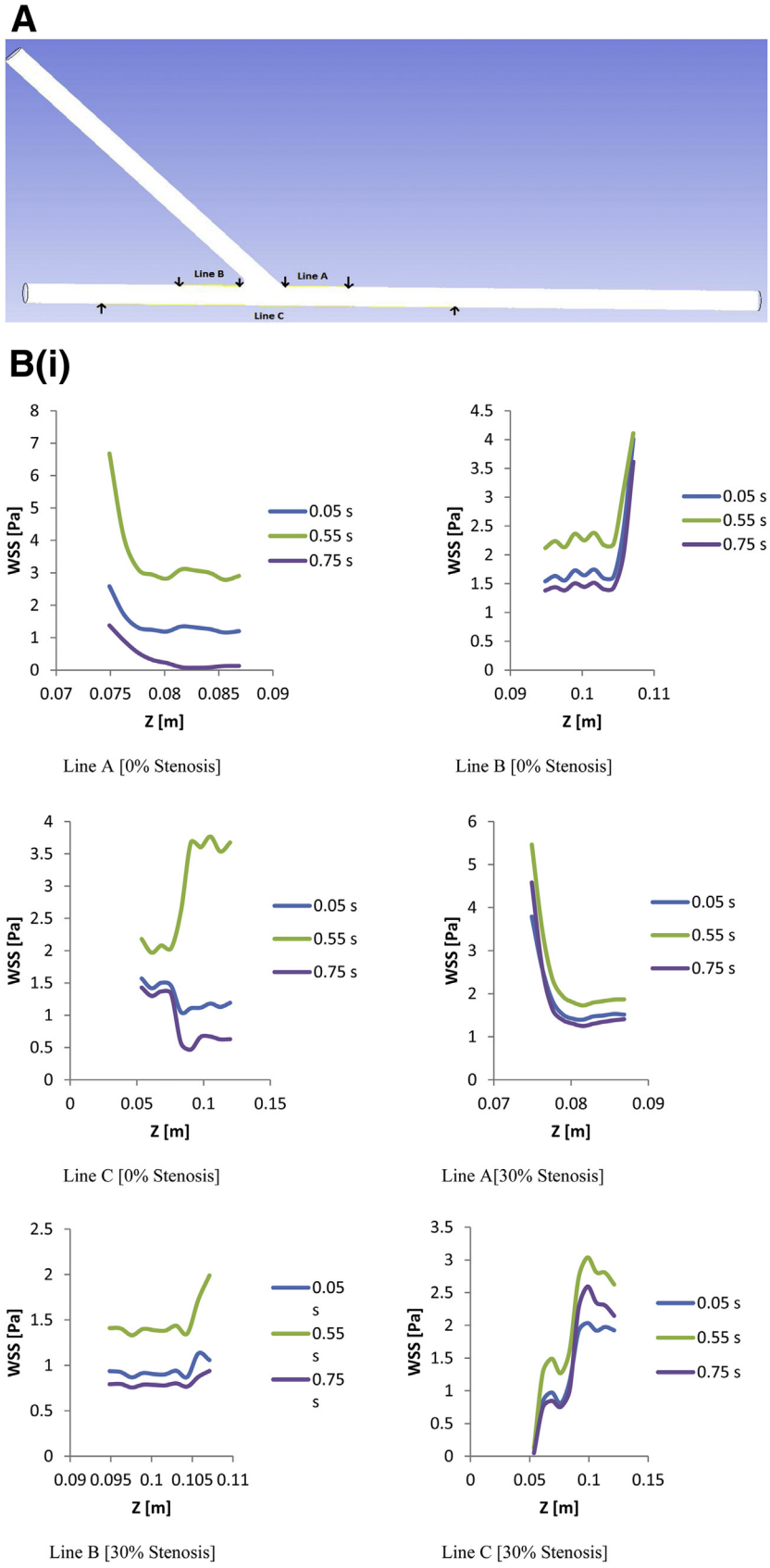

Figure 8. *(A) Line A (WSS distribution at the toe), line B (WSS distribution at heel), and line C (WSS distribution at host bed). (B) Spatial WSS distribution for (i) line A, (ii) line B, and (iii) line C. ITA-LAD = internal thoracic artery–left anterior descending coronary artery; WSS = wall shear stress.*

B(ii)

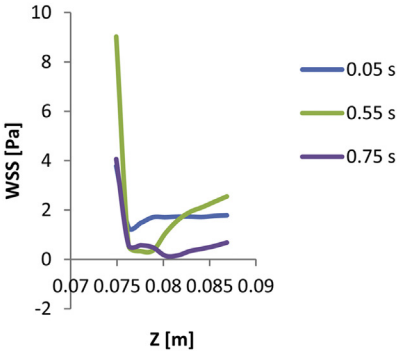

Line A [50% Stenosis]

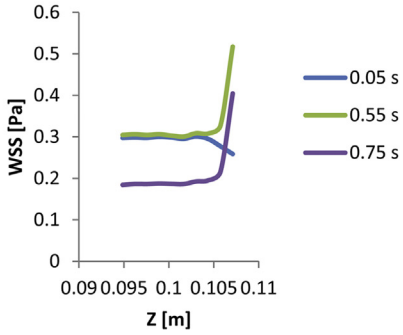

Line B [50% Stenosis]

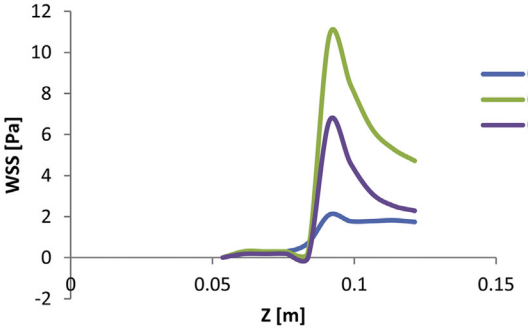

Line C [50% Stenosis]

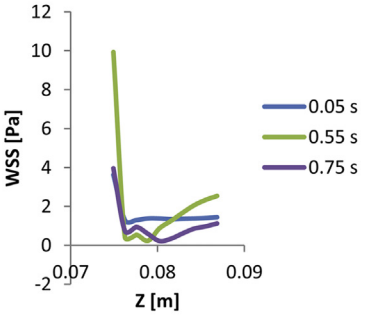

Line A [75% Stenosis]

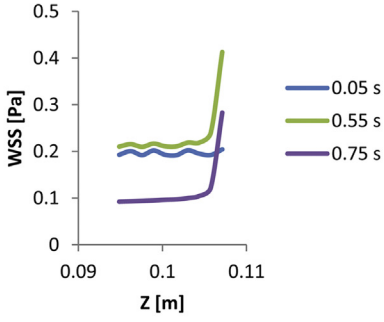

Line B [75% Stenosis]

B(iii)

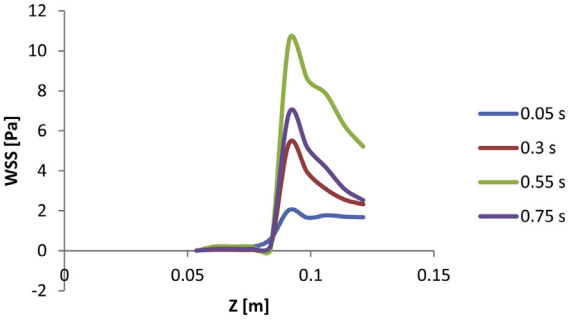

Line C [75% Stenosis]

Figure 8. (continued).

TABLE 3

SPATIAL WSS DISTRIBUTIONS OF THE BYPASS GRAFT FOR DIFFERENT DEGREES OF LAD STENOSIS

% Stenosis	*Observations*
0%	During the time step of t = 0.55 seconds, maximum WSS with the value of 6.8 Pa is found to be from the line A/toe region. Because of higher inflow velocity, higher magnitude of WSS is observed. Precisely, a higher magnitude of inlet velocity entering through the proximal LAD region amalgamates with the flow from the ITA region and results in maximum magnitude of around 6.8 Pa on the toe. In general, from the graphs, higher WSS can be observed because of higher inlet velocity waveforms entering from the ITA and LAD area. Consequently, lower inflow velocities result in lower WSS. Once again, from line B, WSS with the value of around 4.1 Pa is observed to be on the heel of the CABG (t = 0.55 seconds) because of higher inlet flow velocities. Subsequently, from line C during the time step of t = 0.55 seconds, maximum WSS with the value of around 3.75 Pa is observed to be close to the anastomosis area on the bed. However, with the time step of t = 0.75 seconds, lowest magnitude of WSS is observed to be on the anastomosis area of the bed.
30%	With the time step of t = 0.55 seconds for line A, maximum WSS with the value of around 5.4 Pa is observed to be on the toe of the CABG. Again, much higher magnitude of inflow velocities through the ITA and LAD region increased the WSS. Once again, in case of line B during the time step of t = 0.55 seconds, maximum WSS with the value of 2 Pa is observed to be on the heel, and this is because of higher inlet flow profiles. On the other hand, magnitude of the WSS decreases with the decrease in the inlet velocities. Subsequently, with the time step of t = 0.55 seconds WSS of around 3.1 Pa is found to be close to the anastomosis area of the bed (line C) because of higher inflow waveforms. Moreover, because of the stenosis in the proximal LAD, the flow pattern through the host artery is obstructed, which affects the overall flow dynamics and WSS.
50%	The magnitude of WSS around 9 Pa is observed to be on the toe of the CABG for line A with the time step of t = 0.55 seconds. However, due to higher degree of stenosis (50%) in the LAD artery, the flow profiles through the proximal LAD decreased, but higher flow velocity entering through the ITA results in much higher magnitude of WSS on the toe. Likewise, during the time step of t = 0.55 seconds for line B, maximum WSS with the value of around 0.55 Pa is observed to be on the heel, and this is because of higher inlet velocity. In similar time step for line C much higher magnitude of WSS with the value of approximately 11 Pa is observed to be on the bed of the CABG close to the anastomosis area. This can be explained to the fact that higher magnitude of inlet velocity elevates the WSS near the anastomosis area. Moreover, during the time step of t = 0.05 seconds, lowest magnitude of WSS is observed.
75%	Subsequently, during the time step of t = 0.55 seconds, around 10 Pa WSS has been observed on the toe of the bypass graft (line A) due to higher inflow waveform, precisely through the ITA artery. Moreover, for line B (t = 0.55 seconds), WSS with the value of around 0.41 Pa is observed to be close to the heel of the proximal LAD. Again, on the bed of the CABG, WSS with the value of approximately 10.8 Pa is observed (t = 0.55 seconds). Once more, because of increased degree of stenosis in the host artery and minimal inlet velocity, lowest WSS can be observed on the bed (t = 0.05 seconds).

CABG = coronary artery bypass grafting; ITA-LAD = internal thoracic artery–left anterior descending coronary artery; WSS = wall shear stress.

SIMULATION RESULTS

Velocity mapping

Fluid flow characteristics inside the ITA-LAD bypass grafts for different degree of stenosis are illustrated in Figure 6. Velocity vectors that are used to characterize the variation of fluid flow are mapped onto the YZ cross-sectional plane for the total simulation. This proposed cross-sectional plane is taken in the middle portion of the bypass graft as the plane consists of inlets (ITA and LAD), including the anastomosis and the distal area of the host artery. Velocity vectors are illustrated and analyzed for 3 different time steps; at the beginning of the simulation (0.5 seconds), during the middle phase of the simulation (0.55 seconds), and at the end of the simulation (0.75 seconds).[30]

It is understandable that the variation of fluid flows through the proximal LAD and ITA is due to the variation of different inlets. Moreover, with the increase in the degree of stenosis in the LAD artery, the velocity of the fluid flow in the proximal LAD reduces and for the bypass artery (ITA), the flow velocity increases. Due to the difference in the inlet velocities, different

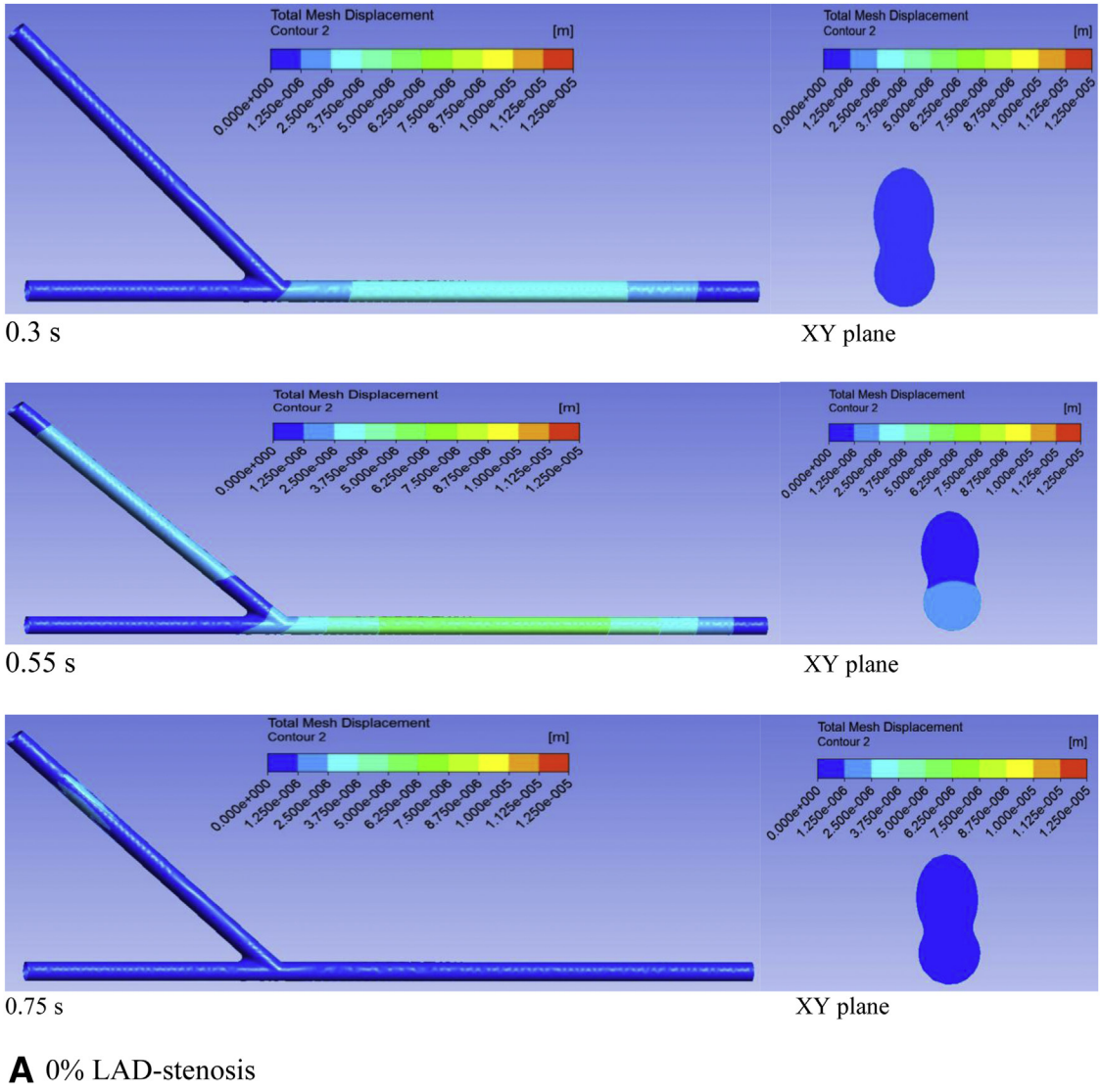

Figure 9. *TMD for the bypass graft and in XY plane for different time steps for the 75% LAD stenosis. LAD = left anterior descending coronary artery; TMD = total mesh displacement.*

outcomes are observed, mostly in the anastomosis region.[30] Results are provided in Table 1.

Distribution of wall shear stress

The variation of the WSS is illustrated in Figure 7 for the 4 different degrees of LAD stenosis in the ITA-LAD bypass graft. The WSS is observed in the fluid region of the bypass graft. Table 2 summarizes the results for the WSS distributions in different time steps.

Spatial WSS distribution. For further analysis on the WSS distributions as documented previously, 3 specific sections of the bypass graft have been highlighted. Specifically, 3 lines (line A, line B, and line C) are selected to study the variations and significance of the spatial WSS. Figure 8A, B show the changes in the WSS for line A (toe), line B (heel), and line C (bed) for 4 different degrees of LAD stenosis. Table 3 represents the findings on spatial WSS distributions based on different degrees of LAD stenosis.

Structural displacement using total mesh displacement

Figure 9 represents the total mesh displacement of the LAD stenosis (0%, 30%, 50% and 75%) in the ITA-LAD bypass graft in various physiological conditions. Changes in the magnitudes of the displacements are determined by using total mesh displacement. It is to be noted that, the variations in the displacements are investigated on the outer surface of the CABG. Subsequently, an XY cross-sectional plane is selected in the anastomosis region, and the changes in the displacement due to the inlet boundary conditions are mapped on to the plane. Table 4 summarizes the overall results of the total mesh displacement during different time steps.

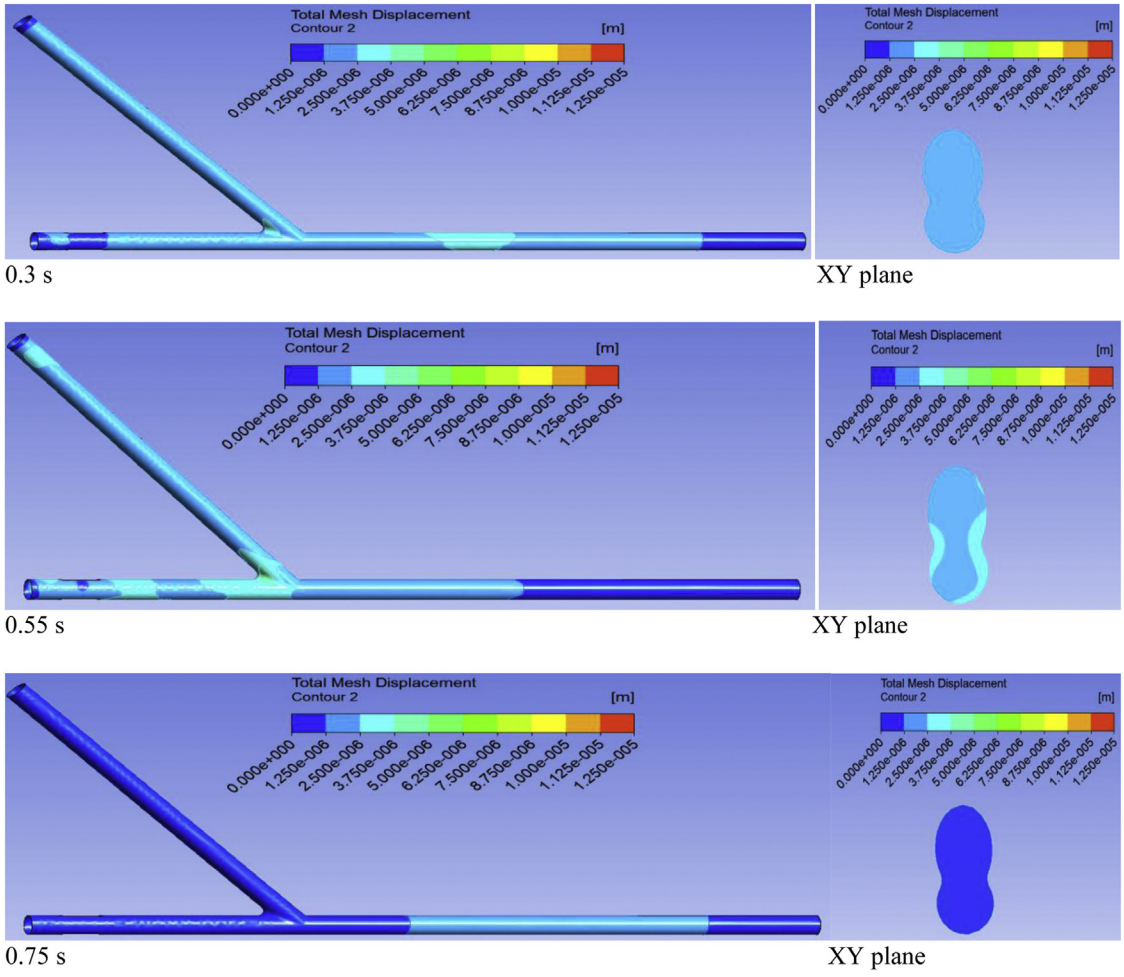

B 30% LAD-stenosis

Figure 9. *(*continued*).*

DISCUSSIONS ON ITA-LAD BYPASS GRAFT FOR DIFFERENT DEGREES OF LAD STENOSIS

Flow pattern inside the bypass graft using velocity vectors

Throughout the simulations, different flow rates are implemented through the ITA and stenosed LAD regions of the CABG to observe and determine the flow pattern inside the bypass graft. Because of variations in the inlet flow velocities, changes in the flow pattern, separation of flow, development of vortices, and other significant phenomena are observed. In addition, simulations demonstrate that the changes in the flow pattern decreased due to higher degree of LAD stenosis.[30]

With the time step of t = 0.05 seconds, reverse flow direction is observed through the ITA section for the 0% LAD stenosis. This can be explained to the fact that, with higher magnitude of inlet velocity through the host artery compared with its graft artery and due to negative velocity gradient through the graft artery, separation of flow and reverse flow in the ITA section is observed. On the other hand, at the same time step, forward-direction flow patterns are observed for the 30%, 50%, and 75% LAD stenosis cases. It is to be noted that, disturbance in the flow velocity is also observed near the heel close to the anastomosis region, for 50% and 75% stenosed LADs.

Subsequently, during the time step of t = 0.55 seconds, the flow pattern is observed to be forward for all stenosis cases. With the rise in the flow velocity through the ITA section and because of the increase in the levels of LAD stenosis, a higher magnitude of flow velocity is observed in the distal LAD region. Specifically, 75% LAD stenosis demonstrated much higher magnitude of velocity than 0%, 30%, and 50% LAD stenosis. In addition, for the 0% and 30%, a smooth flow velocity is witnessed, but for the 50% and 75%, stagnation is observed around the toe near the artery wall (distal LAD). It can be explained to the fact that, because of higher flow profile in the ITA, the flow rate is observed to be higher as well in the distal LAD and because of the anastomosis angle of the graft artery, fluid stagnation is observed near the artery wall. Moreover, due to the supremacy of the flow profile in the graft artery, minor disturbance/obstruction in the flow profile is found to be close to the anastomosis region (75% LAD stenosis), although the

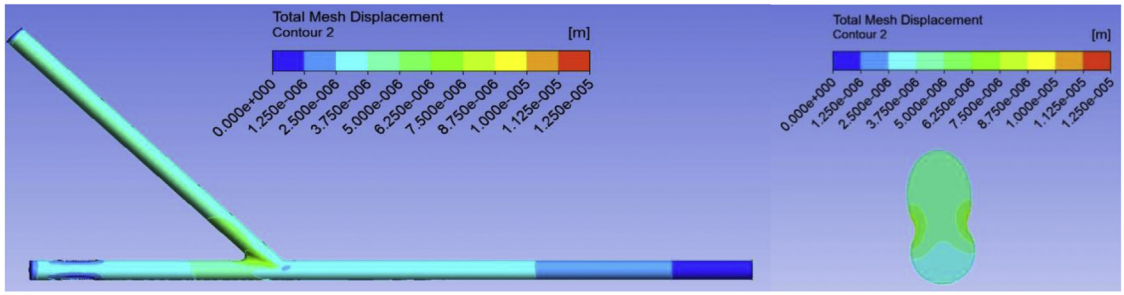

0.3 s XY plane

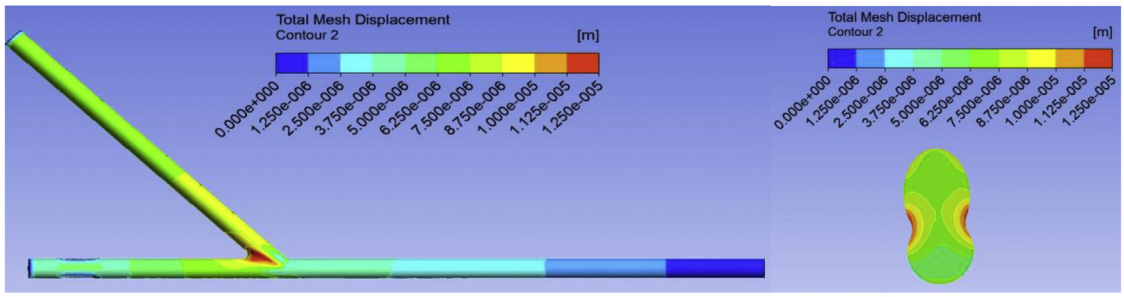

0.55 s XY plane

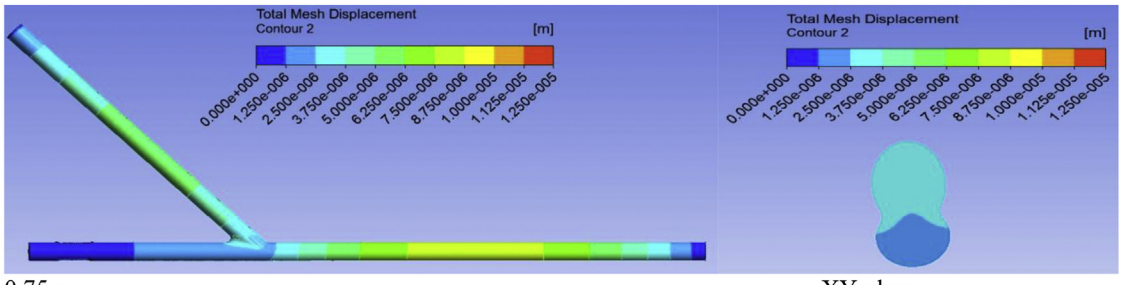

0.75 s XY plane

C 50% LAD-stenosis

Figure 9. *(*continued*).*

flow velocity is minimal through the host artery. In addition, for the same degree of stenosis, previous ring-shaped feeble vortex somewhat mixed with the inflow wave coming from the host artery.

Consequently, during the time step of t = 0.75 seconds, a reversed flow profile is found once more for the no stenosis (0%). This can be attributed to the fact that because of negative inflow wave entering from the graft artery and higher flow velocity coming from host artery, a reversed flow profile is observed in the graft artery. However, forward-direction flow profiles are observed for all the LAD stenosis. For the 30% LAD stenosis, a smooth flow pattern is observed once again in the bypass graft. Moreover, stagnation is also observed close to the artery wall (distal LAD) for 50% and 75% LAD stenosis. In addition, due to lower magnitude of inflow wave through the host artery, the weak vortex which is clockwise and ring-shaped is observed close to the artery wall of the anastomosis area. However, the position of the vortex is moved a little to the distal LAD. The general trend for the flow pattern incorporating the disturbance/separation of the flow, generation, development, merging and shifting of vortices, stagnation, changes in the flow direction inside CABG for all LAD stenosis are in line with the previous investigations/findings.[2,7,30]

Wall shear stress inside the bypass graft using WSS distributions

With the time step of t = 0.05 seconds, the WSS are mainly observed on the LAD (0%), toe (30%, 50%), and ITA (75%). Because of different inlet flow velocities entering through the graft and host artery, WSS changed correspondingly. Precisely, for the 0%/no stenosis much higher magnitudes of WSS are observed on the LAD. With the elevation in the LAD stenosis level, lower magnitudes of WSS are observed on the host artery wall. In addition, the magnitudes of WSS on the toe are observed to be slightly higher for 30% and 50%, but for 75%, somewhat higher magnitude of WSS is observed on the graft artery and close to the toe.

Again, during the time step of t = 0.55 seconds, higher WSS is observed on the LAD region than the ITA due to higher inlet flow waveform (0%). For 30%, WSS is observed to be higher on the distal LAD and toe, but the magnitude of the WSS (distal

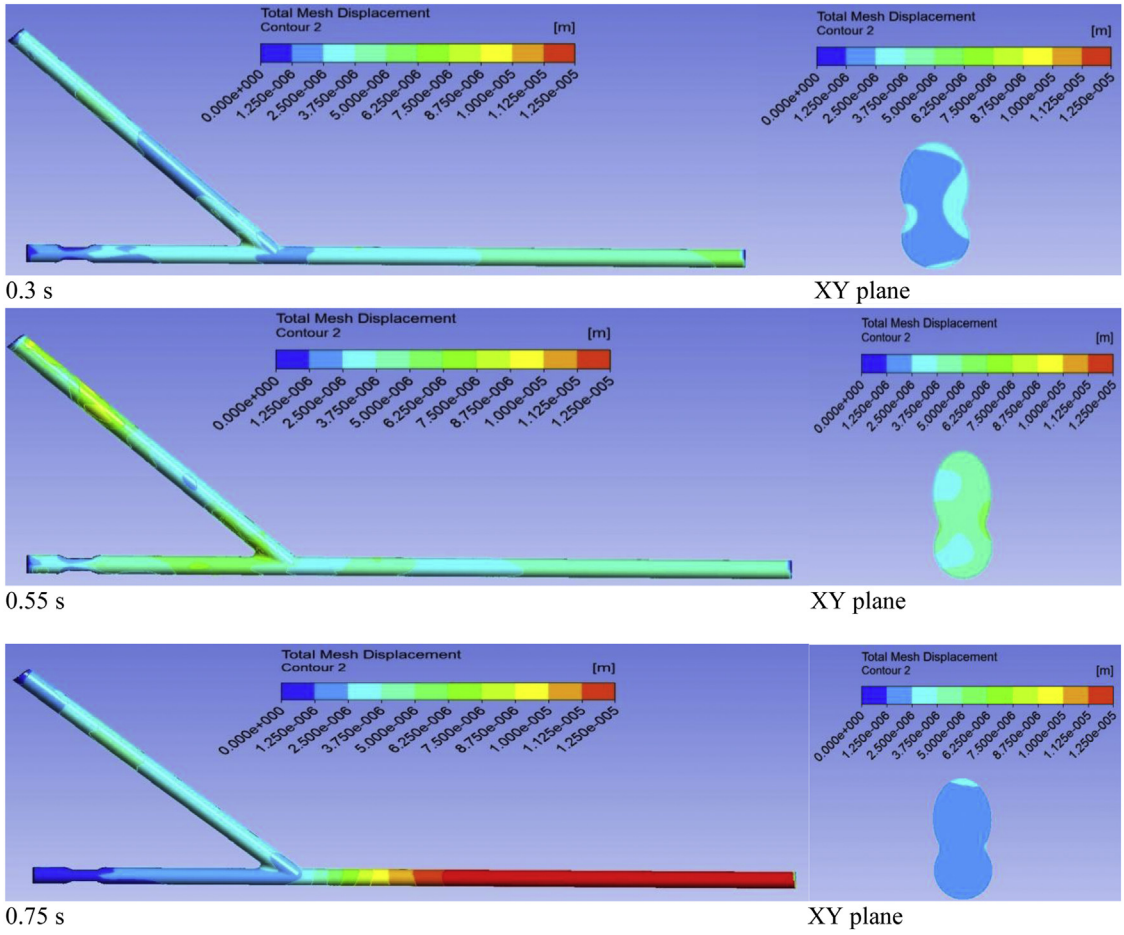

D 75% LAD-stenosis

Figure 9. *(*continued*).*

LAD) is found to be comparatively lower than its 0% LAD stenosis. Precisely, the changes in the inlet flow wave cause the inconsistency on the WSS. Again, for the 50% and 75%, higher inflow flow waveform enters through the graft artery and hence much higher WSS is observed to be on the graft artery, toe, and the distal LAD. It can be explained to the fact that, due to higher stenosis levels and higher inflow waveform entering from ITA, the WSS is observed to be much higher on the toe and close to the anastomosis area of the distal LAD.

Subsequently, with the time step of t = 0.75 seconds, inflow velocity waveform decreased (graft and host artery) for all stenosis levels, and hence, WSS on the bypass graft for 4 different levels of stenosis decreased compared with its time step of t = 0.55 seconds. Moreover, from the simulation results and detailed analysis, it can be stated that the general trend on the changes of the WSS match closely with previously published results.[2,30]

Spatial wall shear stress inside the bypass graft using WSS distributions

The graphical demonstration of the line A (toe), line B (heel), and line C (bed) determines the WSS for various time steps for 4 different LAD stenosis (proximal region). Generally, for 4 different LAD stenoses of line A, maximum WSS is observed close to the toe (t = 0.55 seconds) in the anastomosis region. It can be attributed to the fact that, higher inflow velocity through the graft and host artery is responsible for elevating the magnitude of the WSS (t = 0.55 seconds). However, because of the degree of the stenosis in the host artery, the general flow propagation is hindered, but when the inlet velocity is higher entering through the graft artery (for different LAD stenosis), higher magnitude of WSS can be found on the toe of the artery. Contrariwise, lower magnitude of inflow velocity causes the WSS to be decreased.

Consequently, similar incidents can be found for line B for 4 different degrees of stenosis in the proximal LAD. Once more, due to higher inlet waveform (t = 0.55seconds) maximum WSS can be observed on the heel of the host artery. Although higher WSS is observed in this time step, the results demonstrate that with the rise in the level of stenosis in the proximal LAD, the WSS on the heel is found to be decreased/lower.

Similarly, with the time step of t = 0.55 seconds, maximum WSS is observed on the bed (line C). Once more, higher magnitudes of inlet velocities are responsible for increasing the WSS.

TABLE 4

TOTAL MESH DISPLACEMENT DISTRIBUTIONS OF THE BYPASS GRAFT FOR DIFFERENT DEGREE OF LAD STENOSIS

% Stenosis	*Observations*
0%	Because of the variations in the inlet flow waveforms through the graft and host artery, changes in the displacements are evident. With the time step t = 0.3 seconds, higher magnitude of displacement is observed to be on the distal LAD region. Conversely, due to lower inflow velocity, the magnitude/variations in the displacement are observed to be lower on the ITA and proximal LAD. Again, with further progression in the time step (t = 0.55 seconds) maximum displacement with the value of approximately 6.25E-6 m is observed to be on the distal LAD near the outlet section. In addition, the XY plane shows moderately higher displacement can be observed on the LAD section than ITA. Moreover, due to minimal inlet velocity, the magnitude of the displacement is observed to be lower (t = 0.75 seconds).
30%	With the time step of t = 0.3 seconds, higher magnitude is observed to be on the distal LAD and heel of the CABG. Subsequently with the progression of the time step (t = 0.55 seconds), the magnitudes of the inflow velocities increased through the graft and host artery and because of this, maximum displacement of approximately 3.75E-6 m is observed on the anastomosis area near the heel. In addition, the XY plane demonstrates moderate displacement close to the anastomosis region. However, the magnitudes of the displacements are found to be lower in the graft and host artery and this is because of lower magnitude of inlet velocities. It is to be noted that, moderately higher displacement can be observed on the artery wall of the distal LAD, near the outlet region.
50%	With the time step of t = 0.3 seconds, comparatively higher magnitude of displacement is observed on the heel compared with the ITA and proximal LAD inlets. Because of higher magnitude of inflow wave through the ITA, somewhat higher magnitude of displacement is observed on the heel (XY-plane). Again, with the time step of t = 0.55 seconds, maximum displacement is observed to be around 1.25E-5 m close to the heel due to higher inflow velocity. Moreover, higher magnitude of displacement is observed on the ITA section than the proximal LAD region. After that, with the time step of t = 0.75 seconds, higher magnitude of displacement is observed on the artery wall of the distal LAD region, near the outlet. Also, at the same time, magnitude of the displacement on the ITA is found to be slightly higher than its LAD (XY plane).
75%	With the time step of t = 0.3 seconds, much higher magnitude of displacement is observed close to the outlet. Again, with t = 0.55 seconds, higher displacement value is observed on the heel and on the ITA due to higher inflow velocity coming through the ITA than the stenosed LAD. Finally, during the time step of t = 0.75 seconds, much higher magnitude of approximately 1.25E-5 m is observed on the distal LAD and near the outlet section. At the same time step from XY plane, minimal magnitude of displacement is observed on the anastomosis region because of lower inflow velocity through the inlets.

Moreover, WSS decreased when the inlet waveform decelerates. Once again, the general trends of the changes in the spatial WSS distributions match closely with the previously published results of the study by Kouhi.[2]

Structure simulation of the bypass graft using total mesh displacement distributions

With the time step of t = 0.3 seconds, the magnitudes of inlet velocities are lower for all cases, and therefore, the magnitude of the displacements on the graft and host artery is observed to be minimum. However, somewhat higher displacements are observed on the distal LAD for 4 different levels of LAD stenosis and close to the outlet section (75% LAD stenosis) in this time step. It can be explained to the fact that because of higher inlet velocities through the graft and host arteries, the volume inside the artery increased, and hence, higher magnitudes of displacements are observed.

Consequently, during the time step of t = 0.55 seconds, higher magnitude of inlet velocities coming through the graft and host artery and because of that much higher magnitudes of displacements are observed on the distal LAD (0% LAD stenosis). However, results demonstrate that higher magnitudes of displacements are observed on the heel of the bypass graft for 30%, 50%, and 75% LAD stenosis. Once again, because of higher inlet flow waveforms, volume inside the inlets elevated. Therefore, maximum displacements on the graft and host arteries are found to be for 50%.

Moreover, during the time step of t = 0.75 seconds, inlet velocities decreased for all levels of stenosis when compared with

the time step of t = 0.55 seconds. At this time step (t = 0.75 seconds), lower magnitude of displacement is observed for the 0% LAD stenosis on the entire artery. However, with the rise in the degree of stenosis in the proximal LAD, higher displacement is observed on the distal LAD (30% LAD stenosis), both on the graft artery and the distal LAD (55% LAD stenosis) and maximum displacement close to the outlet section and on the distal LAD (75% LAD stenosis) are observed. This can be explained to the fact that because of lower inlet velocities entering through the host and graft arteries, displacements are observed to be decreased (no stenosis case), and the volume in the artery generates minimal displacement on the artery wall. In addition, for the LAD stenosis (30%, 55%, and 75%), due to the variations of the inlet waveforms entering through the host and graft arteries, volume increased on the graft artery (55% and 75% LAD stenosis) and on the distal LAD (30%, 55%, and 75% LAD stenosis) and hence the magnitudes of the displacements elevated successively.

CONCLUSION

The main focus of this work is to investigate and determine the correlation between the hemodynamic effects with the different degrees of LAD stenosis. Hemodynamic effects including the separation of the flow near the anastomosis region, rapid variation of WSS, and development of vortices are observed different for 4 different types of LAD stenosis. Disturbance of flow is seen only in the anastomosis region, and reverse flow direction is observed for the no-stenosis case but the directions are found to be forward for the 30%, 55%, and 75% LAD stenosis with the time step of t = 0.05 seconds. From the simulations, it is also evident that higher WSS can be found mainly near the toe and on the artery wall, near the anastomosis region. With the increase in inlet velocities, magnitudes of the WSS increase as well. The overall conditions are in line with the previous results and also clinically observed results, which provides a true insight to a large extent. In addition, maximum displacement is observed to be on the distal LAD near the outlet tract (75% LAD stenosis, t = 0.75 seconds). In addition, highest WSS is seen close to the anastomosis region with the value of approximately 1.58E1 Pa, and the structural displacement is found to be around 1.25E-5 m near the heel. In the future, investigations on the effects of the bypass graft using different biomaterials would be carried out to analyze the hemodynamic and the physiological variations including different levels of stenosis. Moreover, experimental studies are being considered by using the combination of particle image velocimetry and Laser Doppler Anemometers, which would truly provide qualitative and quantitative data.

FUNDING

This research did not receive any specific grant from funding agencies in the public, commercial, or not-for-profit sectors.

ACKNOWLEDGMENTS

The author sincerely thanks Prof Yos Morsi and Swinburne University of Technology for constant support and helping him to prepare this manuscript.

REFERENCES

1. Ochi M. Flow capacity of arterial grafts: internal thoracic artery, gastroepiploic artery and other grafts. In: He G-W, editor. Arterial Grafting for Coronary Artery Bypass Surgery; 2006;:279-84.
2. Kouhi E. An advanced fluid structure interaction study of trileaflet aortic heart valve. Melbourne: Swinburne University of Technology; 2011.
3. Mohr R, Kramer A. Left-sided myocardial revascularization with bilateral skeletonized internal thoracic artery. In: He G-W, editor. Arterial Grafting for Coronary Artery Bypass Surgery; 2006.
4. Otaki M, Lust RM, Sun YS, et al. Bilateral vs single internal thoracic artery grafting for left main coronary artery occlusion. Chest 1994;106(4):1260-3.
5. Swillens A, Witte M, Nordgaard H, et al. Effect of the degree of LAD stenosis on "competitive flow" and flow field characteristics in LIMA-to-LAD bypass surgery. Med Biol Eng Comput 2012;50(8):839-49.
6. Sabik JF, Raza S, Blackstone EH, et al. Value of internal thoracic artery grafting to the left anterior descending coronary artery at coronary reoperation. J Am Coll Cardiol 2013;61(3):302-10.
7. Freshwater IJ, Morsi Y, Lai T. The effect of angle on wall shear stresses in a LIMA to LAD anastomosis: numerical modelling of pulsatile flow. Proc Inst Mech Eng H 2006; 220(7):743-57.
8. Owida A, Do H, Yang W, et al. PIV measurements and numerical validation of end-to-side anastomosis. J Mech Med Biol 2010;10(1):123-38.
9. Zhang J-M, Chua LP, Ghista DN, et al. Validation of numerical simulation with PIV measurements for two anastomosis models. Med Eng Phys 2008;30(2):226-47.
10. Kouhi E, Morsi YS, Masood SH. Haemodynamic analysis of coronary artery bypass grafting in a non-linear deformable artery and Newtonian pulsatile blood flow. Proc Inst Mech Eng H 2008;222(8):1273-87.
11. Do HV. Design and optimization of coronary arteries bypass graft using numerical method. Australia: Swinburne University of Technology; 2012.
12. Ethier RC, Steinman DA, Zhang X, et al. Flow waveform effects on end-to-side anastomotic flow patterns. J Biomech 1998;31(7):609-17.
13. Goubergrits L, Affeld K, Wellnhofer E, et al. Estimation of wall shear stress in bypass grafts with computational fluid dynamics method. Int J Artif Organs 2001;24(3): 145-51.
14. Sankaranarayanan M, Ghista DN, Poh CL, et al. Analysis of blood flow in an out-of-plane CABG model. Am J Physiol Heart Circ Physiol 2006;291(1):H283-95.
15. Zarins CK, Giddens DP, Bharadvaj BK, et al. Carotid bifurcation atherosclerosis. Quantitative correlation of plaque localization with flow velocity profiles and wall shear stress. Circ Res 1983;53(4):502-14.
16. Taylor C, Hughes TR, Zarins C. Finite element modeling of three-dimensional pulsatile flow in the abdominal aorta: relevance to atherosclerosis. Ann Biomed Eng 1998;26(6): 975-87.

17. Deplano V, Siouffi M. Experimental and numerical study of pulsatile flows through stenosis: wall shear stress analysis. J Biomech 1999;32(10):1081-90.
18. Bertolotti C, Deplano V. Three-dimensional numerical simulations of flow through a stenosed coronary bypass. J Biomech 2000;33(8):1011-22.
19. Bertolotti C, Deplano V, Fuseri J, et al. Numerical and experimental models of post-operative realistic flows in stenosed coronary bypasses. J Biomech 2001;34(8):1049-64.
20. Cole JS, Watterson JK, O'Reilly MJG. Numerical investigation of the haemodynamics at a patched arterial bypass anastomosis. Med Eng Phys 2002;24(6):393-401.
21. Politis AK, Stavropoulos GP, Christolis MN, et al. Numerical modelling of simulated blood flow in idealized composite arterial coronary grafts: transient flow. J Biomech 2008;41(1):25-39.
22. Perktold K, Rappitsch G. Computer simulation of local blood flow and vessel mechanics in a compliant carotid artery bifurcation model. J Biomech 1995;28(7):845-56.
23. Frauenfelder T, Boutsianis E, Schertler T, et al. Flow and wall shear stress in end-to-side and side-to-side anastomosis of venous coronary artery bypass grafts. Biomed Eng Online 2007;6(1):1-13.
24. Nordgaard H, Swillens A, Nordhaug D, et al. Impact of competitive flow on wall shear stress in coronary surgery: computational fluid dynamics of a LIMA–LAD model. Cardiovasc Res 2010;88(3):512-9.
25. Berger A, MacCarthy PA, Siebert U, et al. Long-term patency of internal mammary artery bypass grafts: relationship with preoperative severity of the native coronary artery stenosis. Circulation 2004;110(11 suppl 1):II36-40.
26. Sankaran S, Esmaily MM, Kahn AM, et al. Patient-specific multiscale modeling of blood flow for coronary artery bypass graft surgery. Ann Biomed Eng 2012;40(10):2228-42.
27. Morsi Y, Owida A, Do H, et al. Graft–artery junctions: design optimization and CAD development. In: Liebschner MAK, editor. Computer-Aided Tissue Engineering. Humana Press; 2012:269-87.
28. Kabinejadian F, Ghista DN. Compliant model of a coupled sequential coronary arterial bypass graft: effects of vessel wall elasticity and non-Newtonian rheology on blood flow regime and hemodynamic parameters distribution. Med Eng Phys 2012;34(7):860-72.
29. Siddiqui SU, Verma NK, Mishra S, et al. Mathematical modelling of pulsatile flow of Casson's fluid in arterial stenosis. Appl Math Comput 2009;210(1):1-10.
30. Ding J, Liu Y, Wang F, et al. Impact of competitive flow on hemodynamics in coronary surgery: numerical study of ITA-LAD model. Comput Math Methods Med 2012;2012:356187.
31. Lassila T, Manzoni A, Quarteroni A, et al. A reduced computational and geometrical framework for inverse problems in hemodynamics. Int J Numer Methods Biomed Eng 2013;29(7):741-76.
32. Temam R. Navier-stokes equations: theory and numerical analysis. American Mathematical Society; UK ed. edition; 2001.
33. Arefin MS, Morsi Y. Fluid structure interaction (FSI) simulation of the left ventricle (LV) during the early filling wave (E-wave), diastasis and atrial contraction wave (A-wave). Australas Phys Eng Sci Med 2014;37(2):413-23.
34. Fluent A. Fluid–structure interaction; 2013. http://www.ansys.com/Products/Simulation+Technology/Fluid+Dynamics/Fluid+Dynamics+Products/ANSYS+Fluent/Features/Fluid%E2%80%93Structure+Interaction. Accessed October 25, 2013.
35. Souli M, Ouahsine A, Lewin L. ALE formulation for fluid–structure interaction problems. Comput Methods Appl Mech Eng 2000;190(5–7):659-75.
36. Huerta A, Liu WK. Viscous flow with large free surface motion. Comput Methods Appl Mech Eng 1998;69(3):277-324.
37. Donea J, Huerta A, Ponthot J-P, et al. Arbitrary Lagrangian–Eulerian methods. Part 1. Fundamentals, Encyclopedia of Computational Mechanics. Hoboken: John Wiley & Sons, Ltd; 2004. https://doi.org/10.1002/0470091355.
38. Lemmon JD, Yoganathan AP. Computational modeling of left heart diastolic function: examination of ventricular dysfunction. J Biomech Eng 2000;122(4):297-303.
39. Patankar SV, Spalding DB. A calculation procedure for heat, mass and momentum transfer in 3-D parabolic flows. Int J Heat Mass Transf 1972;15:1787-806.
40. Lassila T, Malossi ACI, Stevanella M, et al. Multiscale fluid-structure interaction simulation of patient-specific left ventricle fluid dynamics with fictitious elastic structure regularization. Int J Numer Methods Biomed Eng 2012;00:1-23.
41. Olufsen MS. Structured tree outflow condition for blood flow in larger systemic arteries. Am J Physiol Heart Circ Physiol 1999;276(1):H257-68.